Numerical Solution of the Vertical Structure Equation in the Normal Mode Method

Y. K. SASAKI AND L. P. CHANG

Cooperative Institute for Mesoscale Meteorological Studies, University of Oklahoma, Norman, OK 73019

(Manuscript received 24 July 1984, in final form 15 January 1985)

ABSTRACT

In a diagnostic study by expanding global data in normal mode functions, Kasahara and Puri found that for zonal wavenumber one, even the seventh vertical mode (the highest mode they presented) contains about 50% of the energy of the external mode. The vertical normal modes are eigensolutions of the vertical structure equation, and each mode is associated with well-defined physical significance. Consequently, it is of interest to look into the accuracy of representation of, say, the first ten vertical modes in a discretized model because seriously misrepresented normal mode functions may not be able to honestly express the physics embedded in the data to be expanded. Along this line, a systematic method of obtaining matching eigensolutions of the vertical structure equation of a multilayered stratified atmosphere was developed. The resultant eigensolutions were used to investigate the influence of the upper boundary condition, the judicious placement of the vertical grid levels and the relative accuracy of a finite-difference and a finite-element method in obtaining the discretized vertical normal mode functions. An important conclusion of this study is that in a discretized model, an inadequate grid resolution in the upper domain may result in considerable misrepresentation of the vertical structure functions even in the lower part of the domain for vertical modes higher than mode 5.

1. Introduction

In this paper, the normal mode method is regarded as a specific expansion method that uses physically significant eigensolutions of a certain linear system to expand the data variables. In its application to meteorological problems, eigensolutions of the linearized primitive equations are first obtained. These eigenfunctions, also referred to as the normal modes, are then used as basis functions to expand the meteorological variables. Each individual normal mode is associated with a vertical and a horizontal eigenvalue. The merit of the normal mode method lies in the physical significance of the eigenvalues: the vertical eigenvalue can be interpreted as the equivalent depth of a shallow water system and the horizontal eigenvalue the wave frequency.

In the past decade, the normal mode method has found some successful meteorological applications. For instance, Kasahara and Puri (1981) expanded a global data set in normal mode functions and claimed that expansion in normal modes provides better physical interpretation of data than the earlier expansions in empirical orthogonal functions. This close association of individual modes with physics makes the normal mode method an ideal tool for making diagnostic studies of meteorological data.

Another useful application of the normal mode method is to help partition the meteorological variables into the weather-significant rotational waves and the relatively unimportant gravity waves according to the eigenfrequencies of individual modes. Thus, an iterative adjustment of the expanded model variables can be used to find a better-balanced state of the initial wind and mass fields so as to suppress the unwanted high-frequency oscillations in a time-dependent model. This is known as the nonlinear normal mode initialization (see Machenhauer, 1977; Baer and Tribbia, 1977; Puri and Bourke, 1982).

The most important assumption of the normal mode method is the separability of the vertical and the horizontal dependence of the dependent variables of the linearized governing equations. After the separation of variables, the resultant vertical structure equation is solved first to obtain the vertical structure functions; then, for each vertical eigenvalue there is a set of horizontal structure equations to be solved as an eigenvalue problem (Daley, 1981). It is of prime interest to investigate the solution of the vertical structure equation because the subsequent solution for the horizontal structure functions will also depend on the vertical eigenvalues obtained. We will concentrate on the solution of the vertical structure equation in the current paper.

In the aforementioned normal mode diagnostic data analysis by Kasahara and Puri, the total kinetic energy is found to be the largest for the external mode, and, in general, it decreases for higher modes except for the second internal mode. However, vertical modes 4 and 5 still contain substantial amounts of kinetic energy. Even mode 7 contains about half of the kinetic energy of the external mode for zonal

wavenumber one (see Fig. 4 in their paper). They also noted that the amount of kinetic energy contained in the higher modes is much larger than that obtained in earlier studies based on empirical orthogonal functions. Thus, in conducting normal mode data analyses of various scales of motion, it is important to obtain a reasonably accurate representation of a set of discretized normal mode functions, as seriously misrepresented normal mode functions are likely to obscure the physics embedded in the data.

As far as the nonlinear normal mode initialization is concerned, it usually suffices to just initialize the first three or four modes of a typical synoptic-scale model (see Puri and Bourke, 1982). These lower modes are usually well represented by the model's vertical discretization. However, if we consider an accurate prediction of weather in areas of precipitation and potential convective activity, it becomes clear that refined horizontal resolution is required; a mere augmentation of the horizontal resolution without a corresponding refinement in the vertical may have little effect on the overall resolution power of a numerical model (Pecnick and Keyser, 1983). Consequently, as the normal mode initialization is applied to models of finer resolution such as limited-area mesoscale models, in addition to the first three or four vertical modes, one may need to include a few higher vertical as well as horizontal modes in the computation to correctly represent the dynamics and/or physical processes such as the boundary layer processes. In this regard, it is again reasonable to be concerned with the accuracy of the discretized representation of the normal mode functions; i.e., perhaps serious misrepresentation of normal mode functions may result in unrealistic changes in the initialized data.

Even though it is speculated that misrepresented normal mode functions in a discretized model are likely to cause some difficulty in correctly representing the embedded physics, their practical effect on model initialization and on diagnostic study is yet to be determined. This shall be an important subject of an extended study. In the current paper, our aim is to illustrate that insufficient vertical resolution in the upper domain of a discretized model may yield a few considerably distorted normal mode functions for a typical atmosphere. Such a distortion may even reach the lower domain.

Presently, most time-dependent numerical models have no more than twenty vertical layers to span the entire atmospheric column. Because the lowest few kilometers of the atmosphere are observed to contain a significant amount of the total energy of the meteorological phenomena described by the models, it is not uncommon to place most of these affordable grid levels in this lower part of the atmosphere. The presence of the planetary boundary layer in the lower domain of the model further enhances the validity of this arrangement. However, such an arrangement of grids is apt to give relatively coarse resolution in the upper domain, and it needs to be determined whether this leads to misrepresentation of the computed normal mode functions over a large part of the domain. Whatever the answer may be, one needs to be very careful in interpreting the result because there are other factors to be taken into account in choosing the vertical discretization. In a forecasting model, for instance, the choice should be aimed at getting more accurate simulation of the physical aspects of the modeled atmospheric phenomena; it should not be solely determined by how accurately the normal mode functions can be obtained.

The best approach to assessing the accuracy of a numerical solution would be to compare it with a known analytic solution. However, analytic solutions of the vertical structure equation are only available for certain specific stability conditions such as an isothermal atmosphere or an atmosphere of a constant static stability (Jacobs and Wiin-Nielsen, 1966). McFarlane (1971) considered a layer of constant static stability topped by an isothermal layer. By examining the first four modes, he concluded that a forty-level constant-Δp finite-difference method was able to produce fairly accurate vertical structure functions. Without knowing his work, we had conducted a study that was later found to be similar to his work in some respects. However, his work was directed toward the first four modes only, whereas the current study considers the behavior of the higher vertical modes. Some new conclusions that we have reached will be presented in Section 4.

Our method of obtaining closed-form eigensolutions of the vertical structure equation starts by dividing the atmosphere into layers, each of which has its own value of static stability. By requiring continuity of the pressure and the vertical velocity across the interface levels, a matching analytic solution results. The details and the mathematical manipulations of this procedure will be discussed in Section 2. In Section 3, we will explain how discretized solutions of the vertical structure equation can be obtained by a finite-difference and a finite-element method. Discussions of the upper boundary condition to be imposed near the singular point $p = 0$ and the relative accuracy of the two numerical methods will be presented in Section 4. Finally, in Section 5 we will present some important conclusions of our work.

2. Analytic solution of the vertical structure equation

Following the standard procedure (Daley, 1981), the vertical structure equation for a typical primitive-equation model can be written in the pressure coordinate as

$$\frac{d}{dp}\left(\frac{p}{R\gamma}\frac{dZ}{dp}\right) + \frac{Z}{gH} = 0,$$

where Z is the vertical structure function, R the gas constant, γ the static stability parameter $(-(T/\theta)(\partial\theta/\partial p)$, θ being the potential temperature), and H the eigenvalue equivalent depth. As was pointed out earlier, an exact solution to this equation is not available except for a few specific profiles of the static stability. Jacobs and Wiin-Nielsen (1966) and McFarlane (1971) respectively obtained eigenvalue solutions in terms of Bessel functions for an atmosphere having constant static stability and for a constant-stability atmosphere topped by an isothermal layer. In a similar fashion, one may divide the entire vertical domain into a finite number of layers with each layer having its own constant value of static stability. By imposing appropriate upper and lower boundary conditions and requiring continuity of pressure and vertical velocity across each interface level, matching solutions in analytic form can be achieved for such stratifications.

In our opinion, the matching solutions thus obtained represent meaningful approximations to the eigensolutions of a real atmosphere, and hence can be used to test the accuracy of numerical solutions. The reasoning behind this is twofold:

(1) In a numerical model, the temperature profile is only represented at the discretization levels such that the static stability becomes a series of piecewise constant values.

(2) The total number of stratification layers in the multilayered model can be readily increased to better represent a real atmospheric stability profile; the more layers that are used, the more representative the matching solutions become.

In what follows, for the sake of simplicity, we will use a two-layered stratified atmosphere to illustrate how to obtain matching eigensolutions. Similar mathematical manipulations can lead to solutions of multilayered stratifications. The two-layered eigensolutions will also be used to test the accuracy of the numerical solutions of the same stratification. We remark here that a two-layered stratification is only meant to be an idealistic approximation of the gross stability structure of the real atmosphere in which a significant inversion appears near the tropopause. Such a simplified stratification is certainly not expected to represent the detail of a real atmosphere. Nevertheless, it should reflect the major physical structure of the tropopause inversion and provide useful insight into the general structure of the vertical normal modes. Also, a comparison of the single- and double-layered stratifications can reveal what to expect when more layers are used to obtain the vertical normal modes. Note that when the value of the stability parameter remains the same for all layers, the multilayered solution should reduce to the single-layered solution obtained by Jacobs and Wiin-Nielsen (1966).

Referring to Fig. 1 for a two-layered atmosphere, we have as the vertical structure equations

$$\frac{d}{dp}\left(\frac{p}{R\gamma_1}\frac{dZ_1}{dp}\right)+\frac{Z_1}{gH}=0 \quad \text{for Layer 1,} \tag{1}$$

$$\frac{d}{dp}\left(\frac{p}{R\gamma_2}\frac{dZ_2}{dp}\right)+\frac{Z_2}{gH}=0 \quad \text{for Layer 2.} \tag{2}$$

Since γ_1 and γ_2 are constants, the general solution is given by

$$Z_1(p)=A_1J_0[2(m\gamma_1 p)^{1/2}]+B_1Y_0[2(m\gamma_1 p)^{1/2}], \tag{3}$$

$$Z_2(p)=A_2J_0[2(m\gamma_2 p)^{1/2}]+B_2Y_0[2(m\gamma_2 p)^{1/2}], \tag{4}$$

where we have denoted $R/(gH)$ as m for convenience, and this convention will be adopted hereafter. The symbols J_0 and Y_0 represent respectively Bessel functions of the first and the second kind of order zero, and A_1, A_2, B_1 and B_2 are coefficients to be determined by the boundary conditions and the requirements of continuity of pressure and vertical velocity across the interface level. The top boundary condition takes the form of

$$p\frac{dZ_1}{dp}=0, \tag{5}$$

which is derived from $\omega = 0$ at the model top. The lower boundary condition is a result of $w = 0$ at the flat ground surface p_s of temperature T_s. It takes the form of

$$\frac{dZ_2}{dp}+\frac{\gamma_2 Z_2}{T_s}=0. \tag{6}$$

For the interface level p_1, we require continuity of Z and $(1/\gamma)(dZ/dp)$, which are just the dynamic and kinematic conditions across this level. Thus,

$$Z_1(p_1)=Z_2(p_1), \tag{7}$$

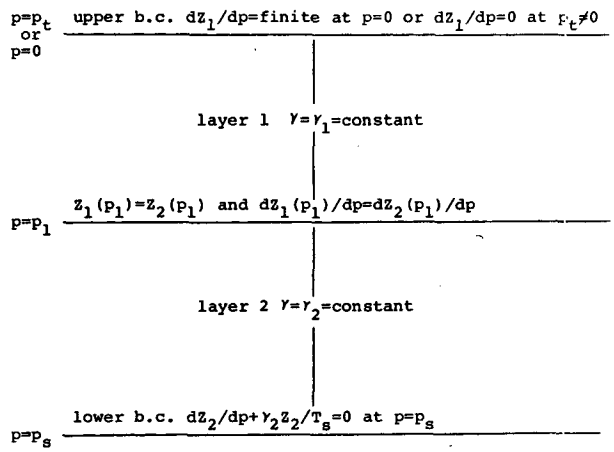

FIG. 1. Schematic representation of the double-layered stratified atmosphere for obtaining closed-form eigensolutions of the vertical structure equation.

$$\frac{1}{\gamma_1}\frac{dZ_1(p_1)}{dp} = \frac{1}{\gamma_2}\frac{dZ_2(p_1)}{dp}. \tag{8}$$

The upper boundary condition (5) can be interpreted as either

$$\frac{dZ_1}{dp} = \text{finite} \quad \text{at} \quad p = 0 \tag{9}$$

or

$$\frac{dZ_1}{dp} = 0 \quad \text{at} \quad p = p_t \neq 0. \tag{10}$$

If we impose (9) as the upper boundary condition, the coefficient B_1 in (3) must vanish, and the other conditions (6), (7), (8) will yield three linear equations in A_1, A_2 and B_2. On the other hand, if (10) is imposed at a nonzero upper pressure level p_t, then four linear equations, in A_1, A_2, B_1 and B_2, will be formed. In either case, the eigenvalues H can be obtained by setting the determinant of the coefficient matrix equal to zero. [Strictly speaking, the eigenvalues are given by $1/(gH)$.] The eigenfunctions corresponding respectively to the upper boundary conditions (9) and (10) are

$$Z_1(p) = B_2'\gamma_2^{1/2}J_0[2(m\gamma_1 p)^{1/2}]\left\{\left\{\frac{-(m\gamma_2)^{1/2}}{p_s^{1/2}}[J_1[2(m\gamma_2 p_s)^{1/2}]Y_1[2(m\gamma_2 p_1)^{1/2}] - J_1[2(m\gamma_2 p_1)^{1/2}]Y_1[2(m\gamma_2 p_s)^{1/2}]\right\}\right.$$
$$\left. + \frac{\gamma_2}{T_s}\{Y_1[2(m\gamma_2 p_1)^{1/2}]J_0[2(m\gamma_2 p_s)^{1/2}] - Y_0[2(m\gamma_2 p_s)^{1/2}]J_1[2(m\gamma_2 p_1)^{1/2}]\}\right\}, \tag{11}$$

$$Z_2(p) = B_2'\gamma_1^{1/2}J_1[2(m\gamma_1 p_1)^{1/2}]\left\{\frac{-(m\gamma_2)^{1/2}}{p_s^{1/2}}\{J_1[2(m\gamma_2 p_s)^{1/2}]Y_0[2(m\gamma_2 p)^{1/2}] - Y_1[2(m\gamma_2 p_s)^{1/2}]\right.$$
$$\left.\times J_0[2(m\gamma_2 p)^{1/2}]\} + \frac{\gamma_2}{T_s}\{J_0[2(m\gamma_2 p_s)^{1/2}]Y_0[2(m\gamma_2 p)^{1/2}] - Y_0[2(m\gamma_2 p_s)^{1/2}]J_0[2(m\gamma_2 p)^{1/2}]\}\right\}, \tag{12}$$

and

$$Z_1(p) = B_1\{Y_0[2(m\gamma_1 p)^{1/2}] - Y_1[2(m\gamma_1 p_t)^{1/2}]J_0[2(m\gamma_2 p)^{1/2}]/J_1[2(m\gamma_1 p_t)^{1/2}]\}, \tag{13}$$

$$Z_2(p) = B_1 b\{Y_0[2(m\gamma_2 p)^{1/2}] + aJ_0[2(m\gamma_2 p)^{1/2}]\}, \tag{14}$$

where B_1 and B_2' are nonzero constants, and the other two constants a and b are defined as

$$a = \left\{\frac{-\gamma_2}{T_s}Y_0[2(m\gamma_2 p_2)^{1/2}] + \frac{(m\gamma_2)^{1/2}}{p_s^{1/2}}Y_1[2(m\gamma_2 p_s)^{1/2}]\right\}\Big/\left\{\frac{\gamma_2}{T_s}J_0[2(m\gamma_2 p_2)^{1/2}] - \frac{(m\gamma_2)^{1/2}}{p_s^{1/2}}J_1[2(m\gamma_2 p_2)^{1/2}]\right\},$$

$$b = \{Y_0[2(m\gamma_1 p_1)^{1/2}] + Y_1[2(m\gamma_1 p_t)^{1/2}]J_0[2(m\gamma_1 p_1)^{1/2}]/J_1[2(m\gamma_1 p_t)^{1/2}]\}/\{Y_0[2(m\gamma_2 p_1)^{1/2}] + aJ_0[2(m\gamma_2 p_1)^{1/2}]\}.$$

When $\gamma_1 = \gamma_2$, Z_1 and Z_2 will reduce to the expressions for the single-layered stratified atmosphere.

3. Discretization of the vertical structure equation

In this section, a finite-difference discretization (Kasahara and Puri, 1981) and a finite-element discretization (Daley, 1978) will be discussed.

a. Finite-difference formulation

Referring to the grid in Fig. 2 (essentially the same as Fig. 1 in Kasahara and Puri), the finite-difference representation of the vertical structure equation becomes

$$\frac{1}{\Delta p_{i+1/2}}\left[\left(\frac{p}{R\gamma}\right)_{i+1/2}\left(\frac{Z_{i+1} - Z_i}{\Delta p_{i+1}}\right) - \left(\frac{p}{R\gamma}\right)_{i-1/2}\left(\frac{Z_i - Z_{i-1}}{\Delta p_i}\right)\right] + \frac{Z_i}{gH} = 0 \tag{15}$$

for $i = 2, 3, \ldots, k-1$, where $\Delta p_i \equiv p_i - p_{i-1}$ and $(\ )_{i+1/2} \equiv [(\ )_i + (\ )_{i+1}]/2$. The upper boundary $p = 0$ or $p = p_t$ is located at level $\frac{1}{2}$ in Fig. 2, therefore, for $i = 1$, the imposition of the upper boundary conditions (9) and (10) yields

$$\frac{1}{\Delta p_{1+1/2}}\left[\left(\frac{p}{R\gamma}\right)_{1+1/2}\left(\frac{Z_2 - Z_1}{\Delta p_2}\right) - 0\right] + \frac{Z_1}{gH} = 0, \tag{16}$$

with $\Delta p_1 = 2(p_1 - p_t)$ where p_t vanishes for boundary condition (9). For $i = k$, application of the lower boundary condition (6) yields

$$\frac{1}{\Delta p_{k+1/2}}\left[\frac{(-p/RT)_s Z_k}{1 + (0.5\gamma\Delta p_{k+1}/T_s)} - \left(\frac{p}{R\gamma}\right)_{k-1/2}\left(\frac{Z_k - Z_{k-1}}{\Delta p_k}\right)\right] + \frac{Z_k}{gH} = 0. \tag{17}$$

The computational levels $\frac{1}{2}$ and $k + \frac{1}{2}$ bring about certain arbitrariness of the choice of Δp_1 and Δp_{k+1}. We will take $\Delta p_1 = \Delta p_2$ and $\Delta p_k = \Delta p_{k+1}$ in all the finite-difference computations.

The system (15), (16) and (17) can be written in matrix form as $\mathbf{AZ} - \lambda\mathbf{Z} = \mathbf{0}$, which can be readily

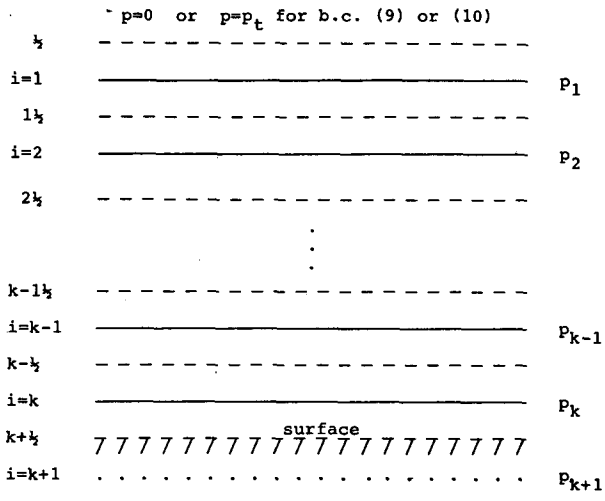

FIG. 2. Finite-difference vertical discretization. Solid lines represent levels at which the vertical structure equation is solved. The $i = ½$ and $i = k + ½$ are employed to help impose the upper and lower boundary conditions.

solved by standard eigenvalue methods. Note that by employing a suitable variable transformation, the coefficient matrix **A** can be made symmetric, which implies that it has all real eigenvalues.

b. *Finite-element formulation*

A finite-element domain discretization is shown schematically in Fig. 3 using linear elements to expand p and Z, and using constant elements to expand γ. By applying the Galerkin method to the vertical structure equation, one gets

$$\left(\frac{p}{R\gamma}\right)_{1+1/2}\left(\frac{Z_{i+1}-Z_i}{\Delta p_{i+1}}\right)-\left(\frac{p}{R\gamma}\right)_{i-1/2}\left(\frac{Z_i-Z_{i-1}}{\Delta p_i}\right)+\frac{(Z_{i+1}+2Z_i)\Delta p_{i+1}}{6gH}+\frac{(Z_{i-1}+2Z_i)\Delta p_i}{6gH}=0. \quad (18)$$

For the boundary levels $i = 1$ and $i = k$, an integration by parts yields

$$\left(\frac{1}{R\gamma}\right)_{1/2}\left(p\frac{dZ}{dp}\right)\Big|_{p_1}-\left(\frac{p}{R\gamma}\right)_{1+1/2}\left(\frac{Z_1-Z_2}{\Delta p_2}\right)+\frac{\Delta p_2(2Z_1-Z_2)}{6gH}=0, \quad (19)$$

$$\frac{p_k}{(R\gamma)_{k-1/2}}\left(\frac{dZ}{dp}\right)\Big|_{p_s}-\left(\frac{p}{R\gamma}\right)_{k-1/2}\left(\frac{Z_k-Z_{k-1}}{\Delta p_k}\right)+\frac{\Delta p_k(Z_{k-1}+2Z_k)}{6gH}=0. \quad (20)$$

It is clear that the boundary term in (19) vanishes for either upper boundary condition (9) or (10).

In matrix form, the finite-element system (18), (19) and (20) can be written $\mathbf{AZ} - \lambda\mathbf{BZ} = \mathbf{0}$ whose solution can be again obtained by standard numerical methods. Here both **A** and **B** are symmetric; consequently all the eigenvalues in the system are real.

In both the finite-difference and the finite-element discretizations, a value of γ weighted from two adjacent grid points will be assigned to the interface level.

4. Results and discussion

In this section, we first investigate the influence of the upper boundary condition on the matching solution of the vertical structure equation. The issue here is the existence of a singularity at $p = 0$. This effect will be studied for both single- and double-layered stability stratifications. The latter will have a stable layer above to simulate the gross physical feature of a tropopause inversion. A comparison of the analytic solutions of these two stratifications may reveal the behavior of the vertical normal modes for a more detailed stability profile. Also, the study of the matching solution under various stability and boundary conditions will pave the way for an investigation of the computational aspects of a discrete model for numerical solution of the vertical structure equation.

It is clear that $p = 0$ is a singular point of the vertical structure equation. The form of the analytic eigensolution varies with whether or not this point is included in the continuous domain as discussed in Section 2. In obtaining discretized eigensolutions, this point can be either included in or excluded from the domain. In general, the farther away from $p = 0$ the top pressure level is chosen to be, the less adverse the effect of the singularity experienced by the discretized solution will be. This point will be explained later.

Following the discussion of Section 2, one may suspect that eigensolutions (13), (14) will asymptotically approach (11), (12) as the top pressure level p_t becomes closer to zero. To clarify this point, values of the equivalent depth H of the ten gravest modes

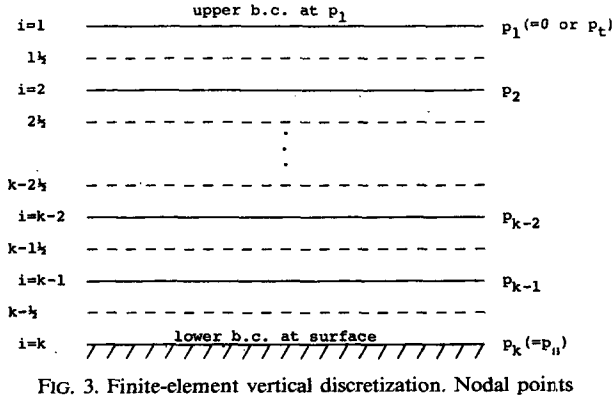

FIG. 3. Finite-element vertical discretization. Nodal points are placed at levels represented by solid lines.

TABLE 1. Analytic equivalent depths in meters of the first ten vertical modes for various upper boundary conditions and stability stratifications. H_1 is the external mode, and all the others are internal modes. The interface level is fixed at 250 mb.

Stability	Upper boundary conditions dZ/dp	Upper boundary conditions p (mb)	Vertical mode H_1	H_2	H_3	H_4	H_5	H_6	H_7	H_8	H_9	H_{10}
	finite	0	9385	308	94	45	26	17	12	9	7	6
$\gamma_1 = 0.04$°C mb^{-1}	0	1	9375	306	93	44	26	17	12	9	7	5
	0	10	9280	291	86	40	23	15	11	8	5	4
$\gamma_2 = 0.04$°C mb^{-1}	0	50	8864	246	68	31	18	11	8	6	4	3
	0	100	8355	197	54	24	14	9	6	5	4	3
$\gamma_1 = 0.25$°C mb^{-1}	finite	0	9619	1097	263	129	86	53	36	28	22	17
	0	1	9605	1083	256	126	83	50	34	27	21	13
Interface 250 mb	0	10	9479	975	216	112	68	40	29	22	16	13
	0	50	8969	642	141	80	39	28	19	13	11	8
$\gamma_2 = 0.04$°C mb^{-1}	0	100	8396	377	108	46	28	17	13	9	7	5

obtained by the analytic solutions are listed in Table 1. An examination of this table shows that for both the one- and two-layered models, the farther away the value of P_t deviates from zero, the more the H-values converge to the H-values obtained for boundary condition (9). It can be seen that the two-layered stratified atmosphere which approximates the gross feature of the tropopause inversion has higher values of the equivalent depth of each mode when compared to the one-layered atmosphere. This implies that a more condensed vertical structure tends to appear in the upper domain in the presence of a tropopause inversion. Therefore, for a fixed discretization mesh, less accurate eigensolutions are to be expected when there is a tropopause inversion, unless the mesh used has very high resolution to resolve all the structures.

TABLE 2. Numerically obtained equivalent depths in meters of the first ten modes of all the figures in this paper. The analytic eigenvalues are also included wherever appropriate for ease of making comparisons.

Stability	Upper boundary p (mb)	Figure number identification	Vertical mode H_1	H_2	H_3	H_4	H_5	H_6	H_7	H_8	H_9	H_{10}
	0	4c	9336	308	93	44	25	15	10	7	5	4
$\gamma_1 = 0.04$°C mb^{-1}		analytic	9385	308	94	45	26	17	12	9	7	6
$\gamma_2 = 0.04$°C mb^{-1}	100	4d	8308	196	53	24	13	8	6	4	3	2
		analytic	8355	197	54	24	14	9	6	5	4	3
	0	4a	9577	1084	252	120	70	39	25	17	11	8
		analytic	9619	1097	263	129	86	53	36	28	22	17
		4b	8358	372	105	44	25	15	11	8	5	3
		7a	8428	388	97	41	15	6	3	/	/	/
$\gamma_1 = 0.25$°C mb^{-1}	100	7b	8392	370	101	44	25	15	8	5	3	2
		7c	8358	374	107	45	27	16	11	8	6	5
Interface level at 250 mb		analytic	8396	377	108	46	28	17	13	9	7	5
		5a	8968	633	140	71	37	23	14	8	5	3
		5b	8984	635	140	76	37	24	16	11	8	6
$\gamma_2 = 0.04$°C mb^{-1}	50	5c	8995	620	140	71	35	20	14	7.2	6.9	4
		6a	9613	965	179	94	49	32	24	18	14	10
		6b	9615	940	186	103	51	39	23	13	9	6
		analytic	8969	642	141	80	39	28	19	13	11	8
*		8a, 2-layer	8358	374	107	45	27	16	11	8	6	5
**	100	8a, b, 3-layer	8449	375	110	47	30	18	13	9	7	5
***		8b, 2-layer	8435	199	57	27	16	10	7	5	4	3

* $\gamma_1 = 0.25$°C mb^{-1}, $\gamma_2 = 0.04$°C mb^{-1}, interface level = 250 mb.
** $\gamma_1 = 0.25$°C mb^{-1}, $\gamma_2 = 0.04$°C mb^{-1}, $\gamma_3 = 0.10$°C mb^{-1}, interface levels = 250, 850 mb.
*** $\gamma_1 = 0.04$°C mb^{-1}, $\gamma_2 = 0.10$°C mb^{-1}, interface level = 850 mb.

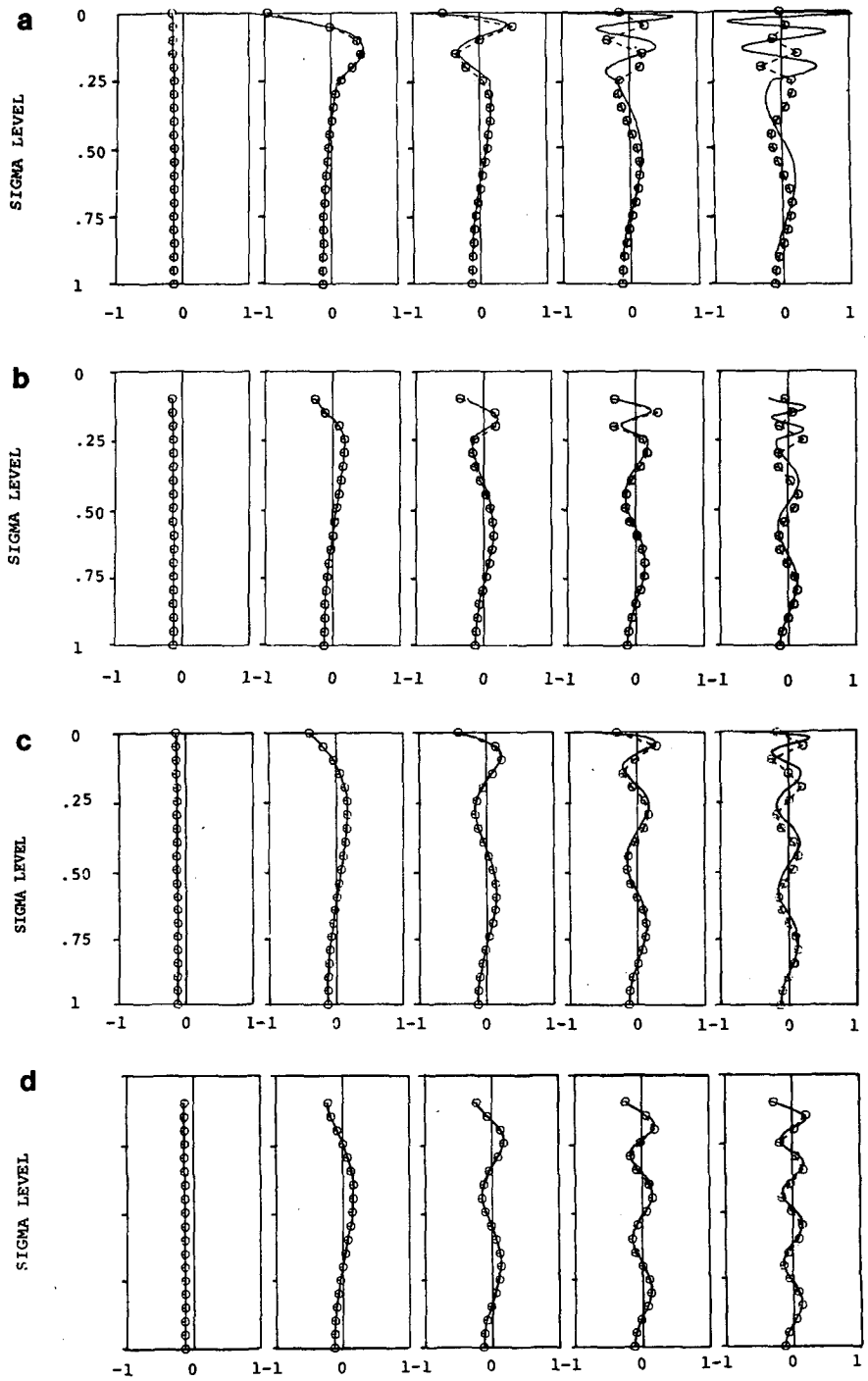

FIG. 4. Finite-element (dashed) and analytical (solid) solutions for eigenfunctions of vertical modes 1, 3, 5, 7 and 9. Circles indicate nodal points used in the discretization. (a) $\gamma_1 = 0.25°C\ mb^{-1}$, $\gamma_2 = 0.04°C\ mb^{-1}$, dZ/dp = finite at $p = 0$, interface level = 250 mb. (b) As in (a) except for $dZ/dp = 0$ at $p = p_t = 100$ mb used as the upper boundary condition. (c) As in (a) except for $\gamma_1 = \gamma_2 = 0.04°C\ mb^{-1}$. (d) As in (b) except for $\gamma_1 = \gamma_2 = 0.04°C\ mb^{-1}$.

For completeness, we list in Table 2 the numerically obtained equivalent depths for all the runs we made in preparing the diagrams for this paper. These values can be compared to the analytical eigenvalues to assess the accuracy of the numerical eigensolutions.

Except the eigenvalues H, the eigenvectors should

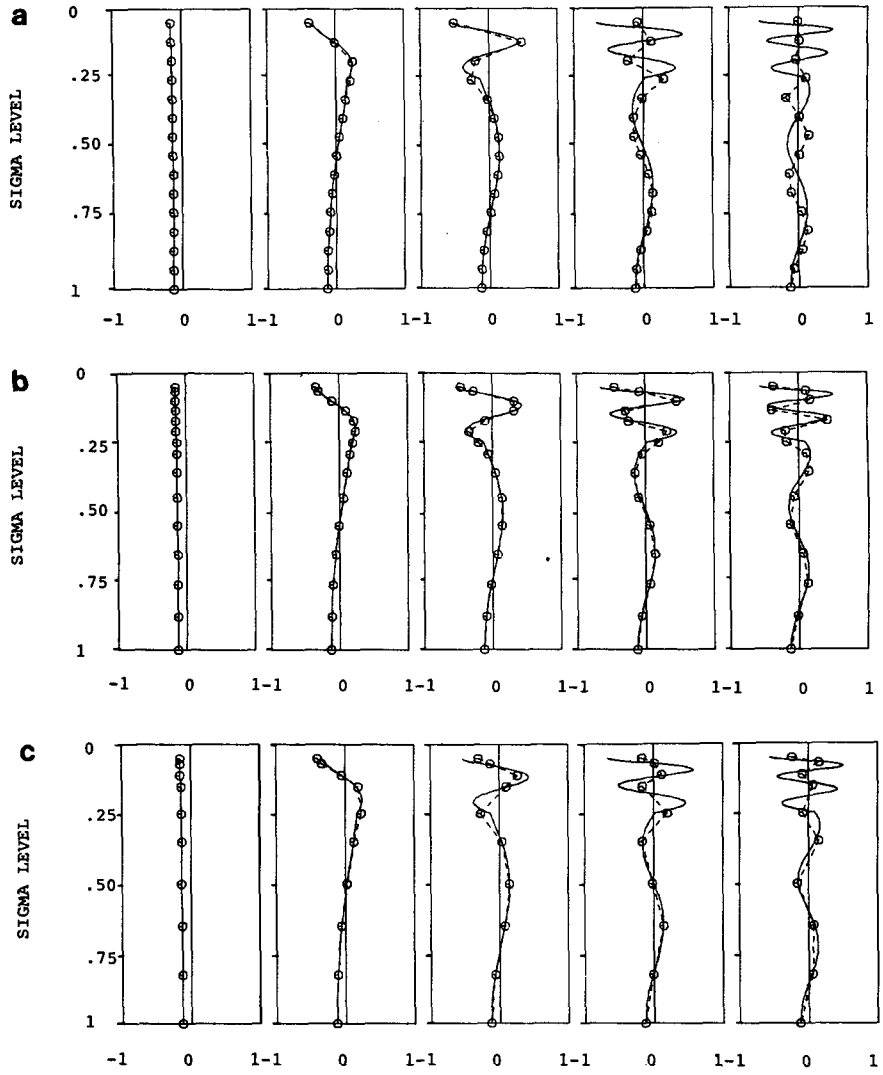

FIG. 5. (a) As in Fig. 4b except for p_t = 50 mb. A constant Δp is used as indicated by the circles. (b) As in (a) except for variable Δp; the same total number of grid points is used in both 5a and 5b. (c) As in (b) except for a total of only ten nodal points instead of fifteen.

also be examined to provide more information on the structure of the vertical normal modes. Since the eigenvectors can only be determined to a multiplicative constant, they need to be normalized to make fair graphical comparisons. In this regard, the surface value of each eigenvector is made equal to a suitably chosen constant before they are plotted. This applies to the analytic as well as the numerical eigenvectors.

The solid curves in Figs. 4a–d give the analytic eigenvectors of modes 1, 3, 5, 7 and 9 plotted on a linear pressure scale. It is clear from these curves that the structures of the vertical modes tend to be more condensed in the upper domain, especially for higher modes. Also, if we compare the results of the single- and double-layered stratifications we find that the stable layer at the top of the two-layered model seems to cause an even stronger packing of structures in the upper domain. This finding corroborates what we found in studying the eigenvalue equivalent depths in Table 1. Another important result is that the application of the upper boundary condition (10) at p_t ($\neq 0$) tends to relax the condensed structures of the higher modes in the upper domain.

Having gained some knowledge of the general behavior of the vertical normal modes from the analytic solution, we may now examine the numerical solutions of the vertical structure equation. To begin with, we used a constant grid spacing of 50 mb in the discrete model to solve for the vertical normal modes. The choice of 50 mb was only meant to be representative of a frequently used resolution in, say, a cloud-scale model. For simplicity, we shall only compare the finite-element solutions with the analytic solutions in most discussions except that of Fig. 6,

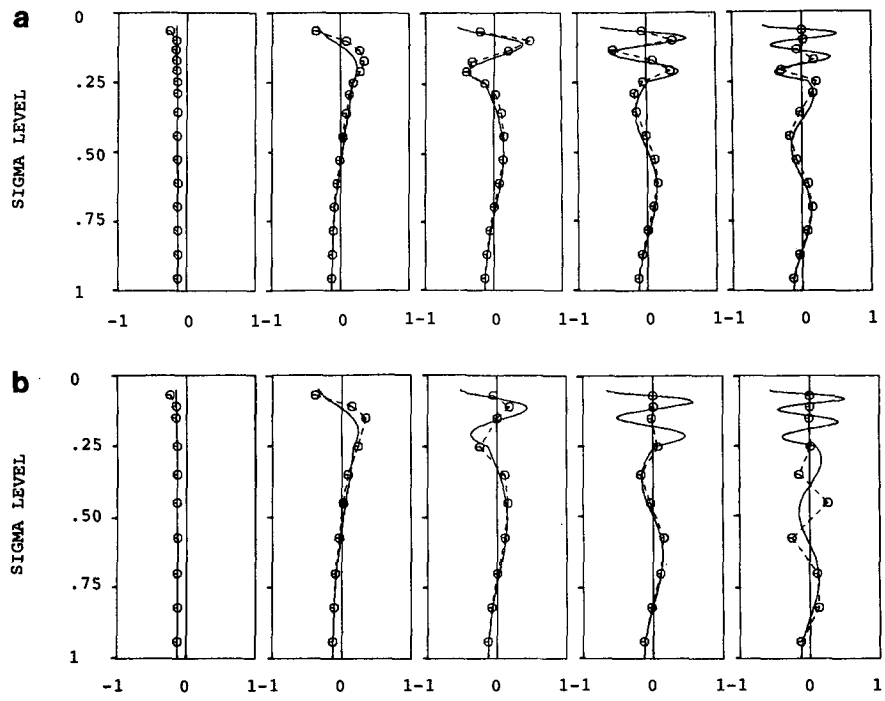

FIG. 6. (a) As in Fig. 5b except that a finite-difference discretization is used.
(b) As in Fig. 5c except that a finite-difference discretization is used.

where a comparison of the finite-difference and the finite-element solutions will be made. The numerical values of the model parameters used in Fig. 4 are: $\gamma_1 = 0.25°C\ mb^{-1}$, $\gamma_2 = 0.04°C\ mb^{-1}$, interface level = 250 mb, model top located at $p = 0$ or $p_t = 100$ mb. The resultant vertical modes 1, 3, 5, 7, 9 are plotted against their corresponding analytic solutions in Fig. 4. By comparing 4a with 4b and 4c with 4d for both stability stratifications, it becomes apparent that the imposition of (10) at $p_t = 100$ mb indeed yields a better overall accuracy than does the use of (9) as the upper boundary condition. Comparisons of 4a, b, c and d also indicate that the two-layered stratification, which roughly simulates the presence of the tropopause inversion, needs to be better represented by using a finer resolution than that used in the one-layered model. We have thus directly confirmed our previous speculation from the study of the analytic solutions.

The condensed vertical structure in the upper atmosphere suggests that maybe a variable grid interval Δp can be used to span the upper domain so as to more effectively resolve the structure of higher vertical modes. To test this out, three different grid configurations were used to solve the vertical structure equation with upper boundary condition (10) imposed at $p_t = 50$ mb. In Figs. 5a and b, the total number of grid points remains unchanged, but Δp is constant in 5a while it is variable with smaller values near the top in 5b. For up to Mode 5, the vertical structure functions are seen to be well represented on both grids, whereas for modes 7 and 9, significantly higher accuracy resulted from the grid of 5b than from the grid of 5a. An important implication of this comparison is that if too coarse a resolution is used to span the upper domain where the vertical structure of higher modes is condensed, then an adverse influence may take place even in the lower part of the domain.

In Fig. 5c, the total number of grid points is reduced from 15, as in 5a, to 10. However, a shrinking of the size of Δp upward yielded a result that compares favorably with that of 5a. This suggests that a judicious placement of grid levels in a discrete model may become critical for obtaining optimal accuracy of the vertical normal modes when higher modes are of importance.

Actually the arrangement of the vertical discretization levels of most primitive-equation models is a rather difficult matter mainly because of the limit of computer capacity. It is common practice to use finer resolution in the lower troposphere where energy sinks and sources appear. Nevertheless, the above results seem to indicate that in order to prevent distortion of the structure of the (higher) normal modes in the lower domain, it is desirable to put adequate resolution in the upper atmosphere. The key here, in our opinion, is an *a priori* estimation of how many vertical modes need to be used in the expansion of model variables. If more modes are involved, higher resolution will be needed in the

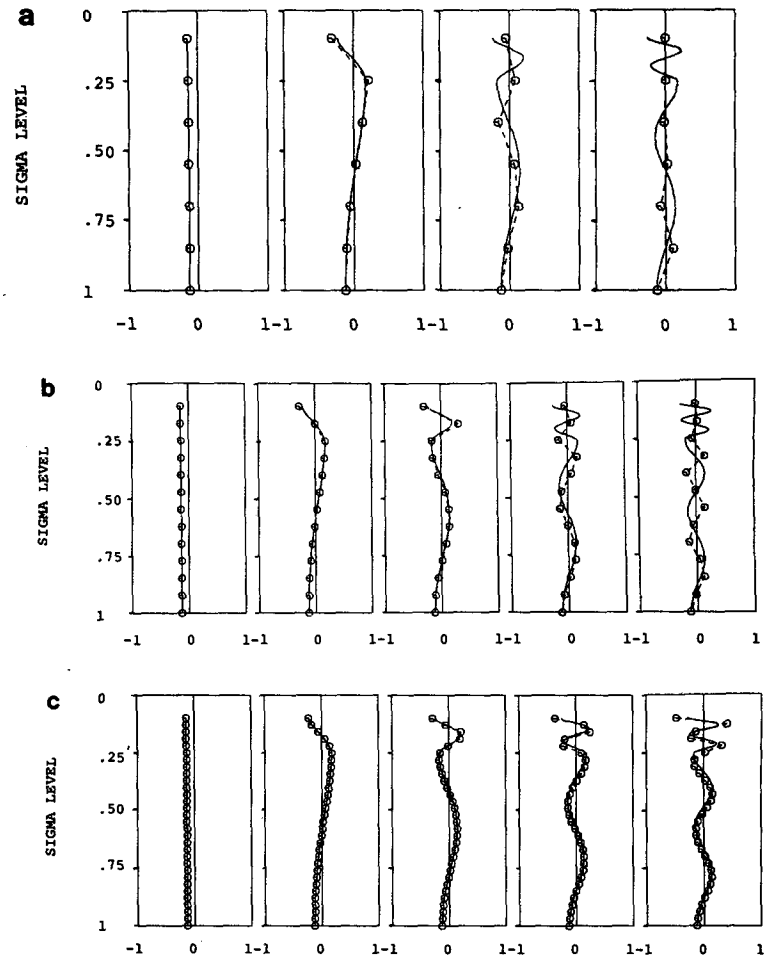

FIG. 7. (a) As in Fig. 4b except that seven grid points are used. (b) As in (a) except that 19 grid points are used. (c) As in (a) except that 31 grid points are used.

upper domain. However, it should be reiterated that the implication of this result should be interpreted with care. For instance, in a forecasting model, the choice of (vertical) discretization levels must be aimed at getting more accurate simulation of the physical aspects of the modeled atmospheric phenomena; it should not be solely determined by how accurately the normal mode functions can be obtained.

Thus far only the finite-element solutions have been compared with the analytic solutions in reaching conclusions about the vertical discretization of solving the vertical structure equation. In order to compare the accuracy of the finite-difference versus the finite-element method for solving for the vertical structure functions, we show in Figs. 6a and b the finite-difference counterpart of the finite-element solutions shown in 5b and c. Because of the different ways of arranging the computational levels in finite-element and finite-difference meshes as evidenced by Figs. 2 and 3, we used the same grid spacings above ~300 mb in both meshes. This, together with the requirement that $\Delta p_1 = \Delta p_2$ and $\Delta p_{k+1} = \Delta p_k$ in the finite-difference mesh, explains why a small Δp appears at the top in Figs. 5b and c. Figures 6a and b show that the finite-difference solutions seem to be "lifted" compared with the analytic solutions. However, more important is that the finite-difference solutions of higher modes, say modes 7 and 9, are considerably less accurate than their finite-element counterparts, as is clear by comparing Fig. 5b with 6a and 5c with 6b. This contrast becomes less significant for mode 7 as the grid resolution becomes refined from the mesh in 5c and 6b to the mesh in 5b and 6a. Thus our use of only the finite-element solutions in reaching major conclusions is justified. This comparison also corroborates the result of an earlier finite-element study by Staniforth and Daley (1977). Since the vertical and horizontal dimensions can be independently discretized, a finite-element grid in the vertical should be considered as a viable alternative to the finite-difference grid when vertical modes higher than Mode 5 are of importance in a model.

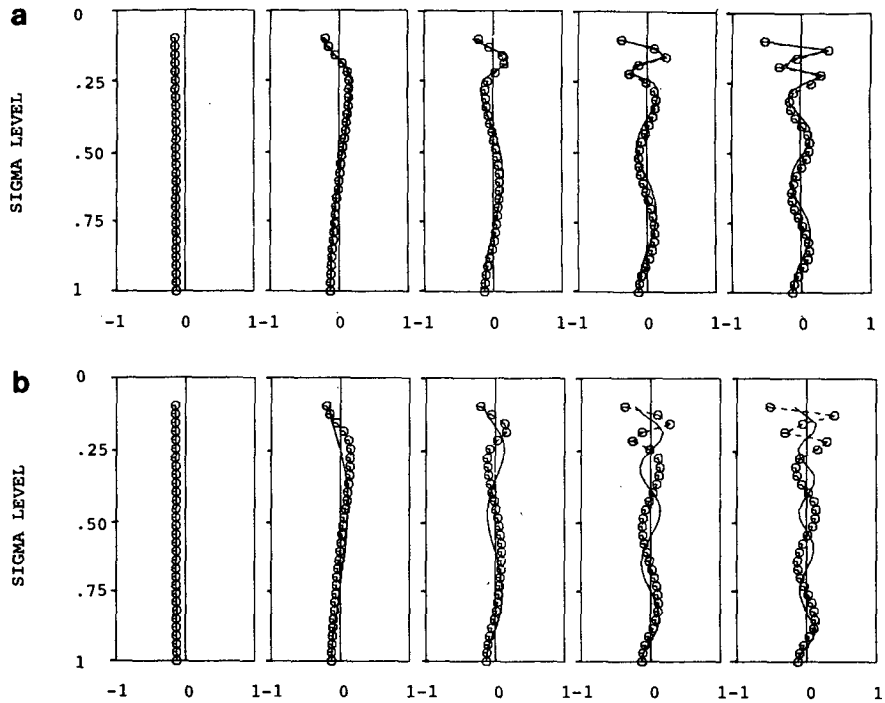

FIG. 8. (a) Comparison of two finite-element eigensolutions. Solid curve represents a two-layered atmosphere as in Fig. 7c. Dash-circled curve represents a three-layered atmosphere with $\gamma_1 = 0.25°C\ mb^{-1}$, $\gamma_2 = 0.04°C\ mb^{-1}$, $\gamma_3 = 0.10°C\ mb^{-1}$, interface levels = 250 and 850 mb. (b) As in (a) except that the two-layered atmosphere now has $\gamma_1 = 0.04°C\ mb^{-1}$, $\gamma_2 = 0.10°C\ mb^{-1}$, interface level = 850 mb.

In the review process, one referee pointed out that Fig. 1 in Daley's (1981) paper suggests that higher modes tend to have significant amplitude only near the earth's surface. However, by examining modes 7 and 9 in Figs. 5 and 6, we felt that the leveling off of the higher normal mode functions away from the surface level is likely an indication of inadequate grid resolution in the upper domain. To formally verify this speculation, we used the finite-element code to test the same case that we studied in Fig. 4b with 21 constant-Δp grid levels. Three runs were made, each having 7, 13 and 31 regularly spaced levels. The results are presented in Fig. 7. An examination of 7a, 7b, 4b and 7c clearly verifies our speculation.

It was also suggested in the review process that the study be extended to a multilayered stratified atmosphere. In order not to obscure the result by having too complicated a stratification, we decided to consider a three-layered atmosphere which is the same as the one considered in Fig. 7c except that a third layer with $\gamma_3 = 0.10°C\ mb^{-1}$ between 850 mb and the surface at 1000 mb is inserted. Because the amount of work involved in obtaining the analytic matching solutions increases drastically with the total number of layers, we think that it is appropriate to use high-resolution, finite-element solutions to study the three-layered atmosphere. The good agreement between the analytic and the finite-element solutions in Fig. 7c using 31 regular intervals justifies our doing so. In Fig. 8a, we plotted modes 1, 3, 5, 7 and 9 for the three-layered atmosphere (solid curves) versus the two-layered atmosphere (dash-circled curves) used in Fig. 7c. This diagram indicates that the presence of a stable layer in the lower atmosphere tends to pull the structure functions toward the surface a little, but its effect does not seem to be able to penetrate the tropopause inversion. On the other hand, as we shall see in Fig. 8b, the presence of a stable layer in the upper atmosphere (the tropopause inversion) seems to have a more extended influence on the lower atmosphere. The solid curves in this figure represent the three-layered atmosphere in Fig. 8a, and the dash-circled curves now represent a two-layered atmosphere with $\gamma_1 = 0.04°C\ mb^{-1}$ between 100 mb (top of domain) and 850 mb, and $\gamma_2 = 0.10°C\ mb^{-1}$ between 850 mb and 1000 mb (surface). Thus, once again, Figs. 8a and b show the effect of a sufficient grid resolution in the upper domain on obtaining accurately represented normal mode functions in a discretized model.

5. Concluding remarks

A model of multilayered stability stratification was devised to obtain analytic eigensolutions of the vertical structure equation: Each layer is characterized by its

own value of the static stability. By requiring continuity of pressure and vertical velocity across each interface level and by imposing suitable upper and lower boundary conditions, matching eigensolutions can be found in terms of the Bessel functions. An explicit example of a double-layered stratified atmosphere was given to demonstrate the mathematical manipulations involved. The resultant vertical structure functions are used to check the accuracy of the numerical solutions by the finite-difference and finite-element methods.

The following conclusions are reached through numerical experiments:

1) In a discretized model, it is beneficial to impose $dZ/dp = 0$ at a nonzero pressure level (say somewhere between 50 and 100 mb) compared to dZ/dp = finite at upper boundary $p = 0$ to alleviate the influence of the singularity at $p = 0$.

2) The general shape of the vertical structure functions suggests the use of smaller values of grid interval Δp to span the upper domain of the model. An inadequate vertical resolution of the upper domain in a discretized model tends to yield misrepresentation of the vertical normal mode functions even in the lower part of the domain, especially for higher modes. In this connection, a vertical coordinate such as $\log p$ may appear to be advantageous to use.

3) The presence of a large temperature inversion above the tropopause produces considerably more condensed structures of the vertical modes in the upper domain compared to the structures of the vertical modes in the absence of the inversion.

4) The finite-element discretization leads to better accuracy than does the finite-difference discretization for solving for the vertical normal mode functions. Therefore, the use of a finite-element vertical discretization in a primitive-equation model deserves serious consideration when higher modes are of importance.

5) The leveling off of the higher normal mode functions away from the surface in a discretized model usually indicates an inadequate grid resolution in the upper domain.

6) A low-level stable layer usually has a more confined effect on the structures of the vertical normal mode functions compared with the effect of an upper-level stable layer (the tropopause inversion).

Acknowledgments. This study was supported by the National Science Foundation Grant ATM-7824892 and the National Aeronautics and Space Administration Grant NAG-5-289 and by the Office of Naval Research Grant N00014-79-C-0758. L. P. Chang wishes to thank the University of Oklahoma for providing the fellowship of the Cooperative Institute for Mesoscale Meteorological Studies. The authors also wish to thank Dr. F. Baer for kindly sending a copy of McFarlane's (1971) project report to us. The helpful comments of the referees are highly regarded.

REFERENCES

Baer, F., and J. Tribbia, 1977: On complete filtering of gravity modes through nonlinear initialization. *Mon. Wea. Rev.*, **105,** 1536–1539.

Daley, R., 1978: The application of non-linear normal mode initialization to an operational forecast model. *Atmos.-Ocean,* **17,** 97–124.

——, 1981: Normal mode initialization. *Rev. Geophys. Space Phys.*, **19,** 450–468.

Jacobs, S. J., and A. Wiin-Nielsen, 1966: On the stability of barotropic basic flow in a stratified atmosphere. *J. Atmos. Sci.*, **23,** 682–687.

Kasahara, A., and K. Puri, 1981: Spectral representation of three-dimensional global data by expansion in normal mode functions. *Mon. Wea. Rev.*, **109,** 37–51.

McFarlane, N. A., 1971: On the numerical evaluation of the structure of various vertical modes in transient planetary waves. Tech. Rep. ORA Project 002630, University of Michigan (Project Director: A. C. Wiin-Nielsen), 33 pp.

Machenhauer, B., 1977: On the dynamics of gravity oscillations in a shallow water model, with application to normal mode initialization. *Beitr. Phys. Atmos.*, **50,** 253–271.

Pecnick, J., and D. Keyser, 1983: The effect of spatial resolution on the simulation of upper-tropospheric frontogenesis using sigma-coordinate primitive equation model. *Preprints, Sixth Conf. on Numerical Weather Prediction,* Omaha, Amer. Meteor. Soc., 134–140.

Puri, K., and W. Bourke, 1982: A scheme to retain the Hadley circulation during nonlinear normal mode initialization. *Mon. Wea. Rev.*, **110,** 327–335.

Staniforth, A. N., and R. Daley, 1977: A finite-element formulation for the vertical discretization of sigma-coordinate primitive equation models. *Mon. Wea. Rev.*, **105,** 1108–1118.